European Journal of Pharmaceutics and Biopharmaceutics 139 (2019) 291–300

Contents lists available at ScienceDirect

European Journal of Pharmaceutics and Biopharmaceutics

journal homepage: www.elsevier.com/locate/ejpb

Research paper

Amorphous agomelatine stabilization in the presence of pyrogenic silica: Molecular mobility and intermolecular interaction studies

Panagiotis Barmpalexis*, Elisavet Vardaka, Ioannis-Minas Moutafidis, Kyriakos Kachrimanis

Department of Pharmaceutical Technology, School of Pharmacy, Aristotle University of Thessaloniki, Thessaloniki 54124, Greece

ARTICLE INFO

Keywords:
Agomelatine
Amorphization
Molecular mobility
Fragility
Relaxation time
Pyrogenic silica
Molecular dynamics simulations

ABSTRACT

In the present work molecular mobility and intermolecular interactions were evaluated as two distinct mechanisms for amorphous agomelatine (AGM) stabilization in the presence of pyrogenic silica. Specifically, amorphous AGM properties related to molecular mobility in terms of relaxation time were calculated based on the Kohlrausch–Williams–Watts (KWW) and Adam-Gibbs (AG) equations, while the kinetic fragility index was calculated based on temperature-modulated differential scanning calorimetry (TM-DSC). Results showed that independently of the approach followed (KWW or AG) AGM's molecular mobility was reduced in the presence of silica (KWW calculated stretched relaxation time constant, τ^{β}, was 83.61 and 44.78 for AGM and AGM/silica dispersions; respectively, while AG-based initial relaxation time, τ^{0}, at storage temperatures 40–50 K below AGM's Tg was increased from six to eight days in the presence of silica); while kinetic fragility index values for amorphous AGM were reduced from 116.05 to 110.24 in the presence of silica. Additionally, MD simulations verified experimentally via attenuated total reflectance (ATR) FTIR spectroscopy, revealed the presence of significant intermolecular interactions between AGM and silica which act as an additional mechanism for amorphous AGM stabilization.

1. Introduction

Nowadays the use of amorphous active pharmaceutical ingredients (APIs) in pharmaceutical formulations has attracted the attention of pharmaceutical formulation scientists [1]. The advantage of such systems over those using the crystalline counterparts is the higher solubility, and hence dissolution rate and bioavailability, which originates from the higher Gibbs free energy due to less favorable intermolecular interactions [2–4]. In addition, the absence of long range molecular order in amorphous materials is the main reason for the observed unique macroscopic properties like mechanical strength and viscosity [5]. In general, amorphous API pharmaceutical formulations, or else amorphous solid dispersions (ASDs) can be prepared by various techniques including solvent-free methods (like hot melt extrusion), 3D printing, freeze-drying, spray-drying, supercritical fluids, electrospinning, electro-spraying and other [6–8]. This wide variety of preparation techniques along with the unique characteristics and advantages of amorphous API based preparations has led to several marketed products, such as Viracept® (nelfinavir), Kaletra® (lopinavir/ritonavir), Indocin® (indomethacin), Sporanox® (itraconazole), Mefoxin® (cefoxitin), Accupril® (quinapril hydrochloride), Accolate® (zafirlukast), Ceftin® (cefuroxime axetil) etc. [9].

A main difference between amorphous materials and their crystalline counterparts is the higher free volume among their molecules and, as a consequence, their higher molecular mobility [10,11]. Practically the molecular mobility of an amorphous material is the inherent structural relaxation including molecular motions like rotation and diffusion which lead to an energetically favorable structure [12]. The evaluation of the above molecular motions and the determination of molecular mobility, which mainly derives from 'aging experiments', helps in the prediction and assessment of amorphous product shelf-life under appropriate conditions and is closely related to the re-crystallization tendency of the amorphous phase [13,14]. Additionally, glass properties of amorphous liquids are closely related to relaxation time and hence, molecular mobility. In general, glass materials are classified as 'strong' or 'fragile' on the basis of fundamental properties like viscosity (η) or relaxation times (τ) around the glass transition temperature (Tg) [15,16]. The viscosity and relaxation time of 'strong' glasses, representing minimal structural changes, follow an Arrhenius like temperature dependence due to tetrahedral networks that are resistant to temperature and structural changes [15], while 'fragile' glass properties deviate significantly from Arrhenius behavior and thus, due to their structure, lack of directional bonds (e.g. aromatic or ionic). Hence, the evaluation of fragility is considered of crucial importance, since it is

* Corresponding author.
E-mail address: pbarmp@pharm.auth.gr (P. Barmpalexis).

https://doi.org/10.1016/j.ejpb.2019.04.015
Received 26 January 2019; Received in revised form 8 March 2019; Accepted 22 April 2019
Available online 23 April 2019
0939-6411/

correlated with the aging behavior and non-exponential relaxation behavior [14,15,17].

Agomelatine (AGM, N-[2-(7-methoxy-1-naphthyl)ethyl]acetamide) is a potent melatonergic agonist (MT1 and MT2) having also 5-hydrotryptamine 2C (5-HT2c) antagonist properties [18]. AGM is a BCS (Biopharmaceutical Classification System) Class II API having low aqueous solubility and high permeability, consisting of a white to almost white crystalline powder that exhibits extensive polymorphism (a total of six crystal forms, named I–VI, have been reported) [19]. In order to enhance its bioavailability the preparation of a new AGM amorphous solid dispersion (ASD) stabilized with the use of a high specific surface area amorphous silica (marketed under the brand name Aerosil®300) was recently reported from our research group [20]. This new ASD system showed remarkably enhanced *in-vitro* dissolution rate as well as *in-vivo* bioavailability (tested in humans) compared to crystalline API-based formulations.

Irrespectively of type (ordered or amorphous), silica offers a high surface area for drug adsorption. The strength of the intermolecular interactions between the adsorbed drug and the silica surface define physical state of the drug (crystalline or amorphous) and its molecular mobility, which in turn controls its rate of release [21]. Therefore, understanding and control of the underlying intermolecular interactions is important in order to enable the design of pharmaceutical products with desirable properties. However, the mechanisms of interaction between the drug and the adsorption surface, are not fully understood. This is mainly due to the high diversity of the surface chemistry of the various grades of silica, which range from fully crystalline to fully amorphous but with different surface density and ionization of silanol groups. The basis of all types of silica is the $(SiO_4)^{4-}$ tetrahedron [22], which forms polymers by linking to self-similar units sharing any number or all of the oxygens of the tetrahedron. A detailed account of the surface chemistry of silica can be found in Vansant et al. [23] or Zhuravlev [24]. The chemical groups found on a silica surface are typically distinguished to siloxanes (also known as Q^4 according the Q^n-terminology used in NMR), single (isolated) silanols (Q^3), and geminal silanols (Q^2), while the presence of vicinal silanols, bridged by hydrogen bonds, is also possible [24]. The number of each group per unit area depends on the method of preparation and thermal treatment of the sample, and in turn defines the hydrophilicity of the surface [23]. Low silanol density is found typically on fumed silica (mainly Q^4 with some Q^3 and even fewer Q^2 surface patches), while exposure to humidity favors the formation of silanol groups by the reaction of the highly strained siloxane groups with water vapor molecules [23]. It becomes clear that there is high variability in the surface chemistry of silicate materials, allowing for a variety of interactions with adsorbate molecules. Computational simulation, such as classical molecular dynamics, can be a very efficient way of investigating these interactions, however the lack of a reliable and realistic way of representation of silica's surface chemistry has been a major obstacle to the successful simulation of molecular adsorption onto silica surfaces [25,26]. Several authors have attempted to describe the surface of silica and construct realistic molecular models of various silica grades, leading to the development of a silica model database [27,28], as well as specialized, accurate force fields for the simulation of molecular adsorption on silica surfaces [29]. Currently, molecular dynamics simulations seem to be a promising method for the study of intermolecular interactions taking place at the surface of silica [30,31].

Therefore, the aim of the present study was to build upon the findings of our previous work (i.e. preparation of a stable AGM-silica amorphous solid dispersion [20]), and gain an insight into mechanisms of amorphous AGM stabilization. Specifically, two distinct mechanisms for AGM amorphous stability will be evaluated: (1) the reduction of API's molecular mobility in the presence of pyrogenic silica (studied in terms of relaxation time and kinetic fragility index), and (2) the possible existence and nature of intermolecular interactions between the API and the carrier, evaluated theoretically via molecular dynamics (MD) simulations and experimentally by ATR-FTIR spectroscopy.

2. Materials and methods

2.1. Materials

AGM (crystal form I) with d(90) of 91.8 mm (measured in Malvern's Mastersizer 2000; Malvern, Malvern, UK) from MSN Pharmachem Pvt. Ltd. (Hyderabad, India) was kindly donated by Rontis Hellas (Athens, Greece). Amorphous silica with specific surface area of 300 m^2/g (Aerosil®300) was obtained from Evonik Industries AG (Essen, Germany).

2.2. Preparation of amorphous samples

2.2.1. Molecular mobility studies

The pure amorphous AGM samples for molecular mobility evaluation were prepared *in-situ* during DSC measurements by heating the initially crystalline API at 10 °C above its melting point maintaining at that temperature for 3 min and subsequently quenching rapidly. No API thermal degradation was observed based on thermo-gravimetric analysis (Shimadzu TGA-50, Shimadzu Corporation, Japan).

Amorphous AGM-Aerosil®300 mixtures for molecular mobility evaluation were prepared by a combination of solvent evaporation method and melt-quenching proposed by Caron et al. [32]. In brief, 1 g of AGM was dissolved in 3 mL of isopropyl alcohol/dichlomethene (ratio 1/1 v/v) at room temperature and kneaded with Aerosil®300 (5.0% w/w) using a mortar and a pestle, until a uniform paste was formed. According to Caron et al., in such studies (i.e. evaluation of molecular mobility in the presence of a carrier) it is important to select a small amount of carrier, since at this level the carrier is not sufficient enough to significantly alter (increase) the Tg value of the API compared to its pure amorphous form (hence the true Tg value to the API is being evaluated instead to the Tg value of the pure carrier), while it is still enough to provide an indication for the changes induced to API's molecular mobility [32]. The wetted paste was dried at 40 °C in a suitable drying oven (Heraeus Noblelight GmbH, Düsseldorf, Germany) until all organic solvents were completely removed (verified by thermogravimetric analysis, Shimadzu, TGA-50, Kyoto, Japan). The recovered powder was then heated *in-situ* during DSC measurements at 10 °C above the melting point of the crystalline API and subsequently quenched in order to ensure that an amorphous sample with no residual crystallinity (verified by DSC) is obtained.

2.2.2. Intermolecular interaction studies

Additionally, an amorphous phase solid dispersion of AGM into Aerosil®300 at a ratio of 50/50 w/w was prepared for the evaluation of possible intemolecular interactions. Briefly, 2.5 g of AGM were dissolved in a 1:1 vol mixture of isopropyl alcohol and dichlormethane, and subsequently mixed manually with Aerosil® 300 using mortar and pestle. After the formation of a paste, the wet-kneaded mass was dried at 60 °C for 3 h in a Heraeus UT 12 forced convection drying oven (Heraeus Noblelight GmbH, Düsseldorf, Germany) and stored in a desiccator before further testing.

It is important to note that API's chemical instability may also occur during the preparation process of the silica-AGM ASD (e.g. solvent and heat exposure, mechanical stress etc.). However, since the aim of the present study was to evaluate the mechanism of API's amorphous stability, the chemical degradation of AGM was not evaluated.

2.3. Molecular mobility studies

All DSC thermograms were recorded using DSC 204 F1 Phoenix heat-flux differential scanning calorimeter (NETZSCH, Selb, Germany) after temperature and enthalpy calibration using indium. Specifically, accurately weighted samples (3–5 mg) of AGM and AGM-Aerosil®300

were placed in perforated aluminum pans under a nitrogen gas flow of 75 mL/min and the thermic events (i.e. glass transition (Tg), crystallization (Tc), melting (Tm) temperatures etc.) were recorded. Specifically, Tg was defined as the midpoint of the change in heat capacity of the sample, while both Tc and Tm were defined using the peak temperatures of the recorded exothermic and endothermic peaks, respectively. The standard deviations of temperatures determined in this work were not higher than 1.0 °C.

2.3.1. Determination of relaxation time

In general, molecular mobility is determined as the reciprocal of the relaxation time (τ). There is no single equation to calculate the relaxation time since all proposed models make several unique assumptions; however, the two most commonly used equations in pharmaceutical applications, that give an indication on the mobility within an amorphous sample are the KWW and the AG equations [33].

2.3.1.1. KWW approach. AGM molecular mobility was evaluated with the aid of KWW approach which assumes that the relaxation time of a sample can be determined by measuring the enthalpy lost during annealing process [33–36]. Based on KWW, when an amorphous API relaxes it loses some of its excess thermodynamic properties such as enthalpy, and hence upon reheating the recovered enthalpy may be visualized in the DSC as an enthalpic overshoot at Tg.

In the present study, for the determination of relaxation time (and hence molecular mobility) the DSC *in-situ* prepared amorphous AGM and AGM- Aerosil®300 samples were kept at −28 °C for 0, 2, 4, and 8 h prior to re-heating with 10 K/min. The relaxation enthalpy was calculated by the estimating the relaxation endotherm in Tg from the following equations:

$$\varphi(t) = 1 - \frac{\Delta H_{relax}}{\Delta H_{\infty}} = exp\left[-\left(\frac{t}{\tau_{KWW}}\right)^{\beta}\right] \quad (1)$$

$$\Delta H_{\infty} = \Delta Cp(Tg - T) \quad (2)$$

where $\varphi(t)$ is relaxation function, ΔH_{relax} is enthalpic relaxation, ΔH_{∞} is maximal theoretical enthalpic relaxation, t is time, τ_{KWW} is relaxation time, β is stretched exponential parameter ($0 < \beta < 1$), ΔCp is heat capacity change at Tg, and T is the aging temperature.

2.3.1.2. AG approach. Additionally, molecular mobility of amorphous AGM was determined based on the AG approach (also known as also known as the Adam-Gibbs-Vogel equation), by evaluating the dependence of Tg on the heating rate of the amorphous phase. Specifically, neat AGM and AGM- Aerosil®300 samples were heated 10 °C above their melting temperature, equilibrated for three min in order to achieve complete melting (delete of thermal history) and then subsequently supercooled to −60 °C (at 200 K/min cooling rate) and equilibrated for three min, before heating again to 30 °C above their Tg at several heating rates (namely, 5, 10, 15 and 20 K/min).

In this approach, the concept of configurational entropy is taken into account when determining the relaxation time [33,34,37,38]. During relaxation the enthalpy and entropy of the amorphous glass is reduced resulting in a configurational entropy which is dependent on both temperature and time. In one of its forms, the AG equation is written as [33]:

$$\tau^0 = \tau_o exp\left(\frac{DT_o}{T(1 - T_o/T_f)}\right) \quad (3)$$

where, τ^0 is the relaxation time, τ_o is the pre-exponential parameter ($=10^{-14}$ s), D is Angell's strength or fragility parameter, T_o is temperature of zero configurational entropy (where no structural mobility occurs) and T_f is fictive temperature (the temperature at which the observed properties of a glass correspond to that of the equilibrium state). A step-by-step process for estimating the required values is given in the published work of Mao et al. [39].

2.3.2. Determination of fragility via TM-DSC

In addition to the AG fitting described above, where fragility of the samples was determined by parameter D, in the present study the kinetic fragility was also evaluated via TM-DSC [40]. The use of modulation in DSC measurements as proposed by Chakravarty et al. [15] enables the complete separation of reversing (Tg) and non-reversing events (ΔH), thereby resulting in improved baseline and greater reproducibility for measured fragility values. Specifically, after the *in-situ* preparation of amorphous AGM and AGM- Aerosil®300 samples described in Section 2.2, the quench cooled samples at −38 °C were heated to 25 °C and then cooled again at −38 °C with different cooling rates (namely 0.25, 0.5, 2, 5, 10 and 20 K/min). The kinetic fragility was calculated by re-heating the samples at a heating rate of 2 K/min, with a period of 60 s and an amplitude of ± 1 °C. The 2 K/min cooling scan rate was chosen as the standard scan. ΔH(Q) obtained from the difference in ΔH between the standard scan and the rest was used to determine the fictive temperature, T_f, and Eq. (4) was used for the numerical estimation of fragility:

$$\log\left(\frac{Q}{Q_s}\right) = m - m\frac{T_f^s}{T_f} \quad (4)$$

where, Q and Qs are the cooling rates for the employed and the standard (denoted with an "s") scans, m is the fragility index (which is the "steepness" of the viscosity/relaxation time versus temperature curve as T approaches Tg) while T_f and T_f^s are the fictive temperatures of the employed and the standard scans, respectively.

2.4. Intermolecular interaction studies

2.4.1. MD simulations

MD simulations were used in order to evaluate the presence of intermolecular interactions between AGM and Aerosil®300. The construction of a realistic model for the simulation of silica is not a trivial task, due to the high diversity in the surface chemistry, depending on the type of silica that is being simulated. In our case, Aerosil® 300 belongs to the class of pyrogenic or fumed silica, produced by a flame-hydrolysis procedure. According to the manufacturer's technical data sheet (https://www.aerosil.com/sites/lists/RE/DocumentsSI/Technical-Overview-AEROSIL -Fumed-Silica-EN.pdf), Aerosil consist of aggregates of primary amorphous particles with mean diameter ~12 nm, forming branched aggregates of 200 nm maximum diameter. This structure gives rise to a very high specific surface area that, in the case of Aerosil® 300 has been found equal to 295 m^2/g, corresponding to a volume of 0.56 cm^3/g of pores between 2 and 100 nm. A very important feature of fumed silica in general, and of Aerosil® 300 in particular, is its low silanol group density, which is reported to be between 1 and 1.5 free silanol groups/nm^2.

Several researchers have attempted to simulate ordered and amorphous silica, which has led to the development of databases of realistic models of the various silica types, such as the ones provided by Enami et al. [27] and Ugliengo et al. [28]. For the purposes of our study, the most suitable model appears to be the amorphous silica model with 1.5 silanol/nm^2, which is included in the dataset proposed by Ugliengo et al. [28] because it closely matches the structure of the pyrogenic Aerosil® 300. The model of amorphous silica was based on a cristobalite cubic cell, heating up to 6000 K and cooled down to 300 K by a molecular dynamics run before being energy-minimized by periodic B3LYP calculations.

The INTERFACE force field parameters [27] embedded in the PCFF force field, along with the corresponding partial atomic charges were used for the silica surface slab, while for agomelatine INTERFACE parameters and partial atomic charges calculated by the charge equilibration method known as Qeq [41], were employed.

A 3 × 3 × 1 supercell was constructed from the original surface model with dimensions a = 37.29800 b = 39.36480 c = 50.00000 and α = 90.00000 β = 90.00000 γ = 87.99050, and a "droplet" consisting of six randomly aggregated agomelatine molecules was placed at the center of the surface. The selection of the supercell size was considered to be sufficient, since its dimensions exceeds the force field's cutoffs for calculation of the various interactions. Additionally, since periodic boundary conditions (PBC) were applied, the simulation box's size is, theoretically, infinite. Simulation's computational time for each 1.5 ns run (three runs were performed totally in order to evaluate the repeatability of simulations) lasted for a couples of days. Computation time in this kind of simulations usually scales exponentially with system size, and hence, increasing the supercell size will require extreme computational power. For the MD simulations, after energy minimization and a short equilibration period, a production run followed for 1.5 ns using the NVT ensemble at 298 K (meaning that the number of atoms, the volume and shape of the simulation box as well as the simulation temperature were kept constant), with Andersen thermostat and a time step of 1 fs. The center of mass was fixed, the cut-off radius was set at seven (7) Å, while the spline distance and buffer thickness was set at one (1) Å each. The number of preliminary equilibration steps was set at 1000 with data output collected every 10 steps. In order to ensure the validity of the simulations, the criteria suggested by van Gunsteren and Mark were taken under consideration in model development, force field selection, sampling scheme setup, and software selection/usage [42].

The Xenoview ver. 3.8.1 (http://www.vemmer.org/xenoview/xenoview.html) was used for the calculations, and the VMD [43] (https://www.ks.uiuc.edu/Research/vmd) and Multiwfn [44] software programs for the analysis of trajectory data, and for the visualization of intermolecular interactions.

2.4.2. ATR-FTIR spectroscopy

In order to experimentally verify the intermolecular interactions suggested by MD simulations, attenuated total reflectance Fourier-transform infrared spectroscopy (ATR-FTIR) was employed. Specifically, FTIR spectra in the region of 600–3600 cm^{-1} for both AGM polymorphs (i.e. Form I and II) and Aerosil®300, along with the prepared solid dispersions (at a ratio of 50/50 w/w API to Aerosil®300) were obtained using a Shimadzu IR-Prestige-21 FTIR spectrometer coupled with a horizontal Golden Gate MKII single-reflection ATR system (Specac, Kent, UK) equipped with a ZnSe lens, after appropriate background subtraction. Sixty-four scans over the selected wave number range at a resolution of 4 cm^{-1} were averaged for each sample.

2.5. Statistical analysis

DSC results were evaluated for statistical significance using student's *t*-test for differences between two group means. The confidence level for statistical significance was set at a probability value of 0.05. Comparison of DSC results for pure AGM and AGM/silica samples showed statistically significant differences ($p < 0.05$) in the measured parameters.

3. Results and discussion

3.1. Molecular mobility studies

In general, the excess entropy, enthalpy and free energy of the amorphous phase (compared to crystalline counterparts) play a crucial role in re-crystallization behavior. The once common practice of storing the amorphous APIs or API formulations at temperatures 50 °C below their Tg was quickly abandoned as it was realized that recrystallization may still occur at these temperatures [45]. Therefore, a thorough evaluation of molecular mobility is a prerequisite for the successful development of an effective amorphous drug formulation with acceptable storage stability (at least during shelf-life), as well as for gaining insight into the mechanism of the API's recrystallization process. In order to evaluate molecular mobility at and below Tg, DSC studies of relaxation time and glass fragility have been proposed [17].

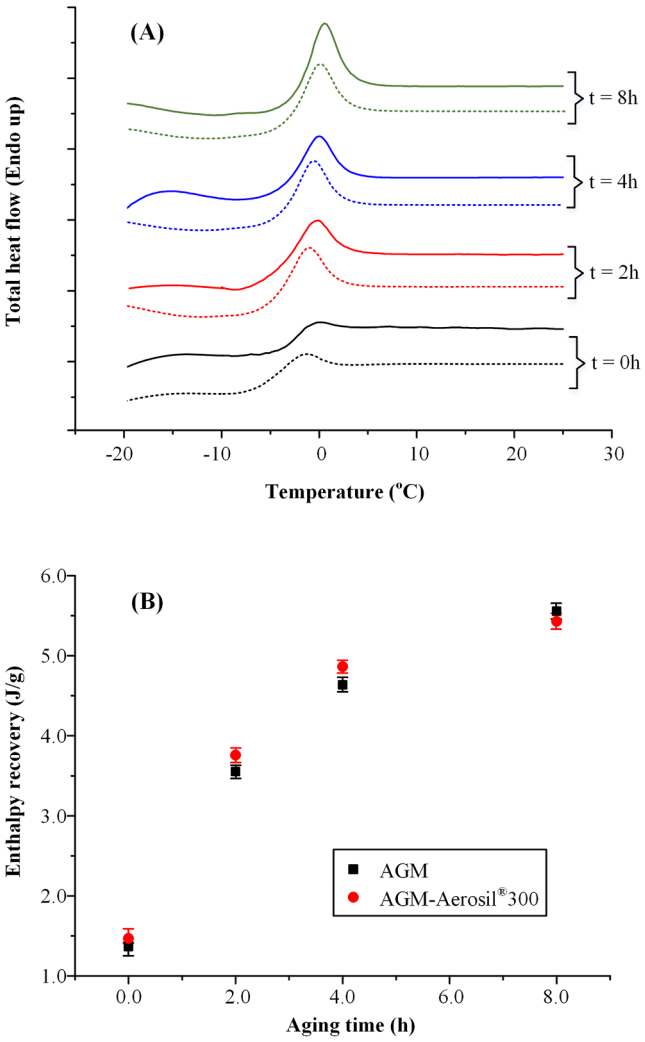

Fig. 1. (A) Relaxation DSC enthalpic overshoot (full line depicts AGM while dashed lines depict AGM-Aesosil®300 mixtures); and (B) Enthalpy recovery values at Tg for the quench-cooled AGM, annealed for different time lengths.

3.1.1. Relaxation time

In amorphous pharmaceutical solids the reliable estimation of molecular mobility should take into account the non-exponential and non-linear nature of structural relaxation. Hence, as the available approaches are not capable of accounting for either, it is suggested to employ simultaneously the KWW and AG equations which address the non-exponential and non-linear assumptions, respectively [46].

3.1.1.1. KWW fitting. Fig. 1(A) and (B) illustrate the DSC thermograms and the enthalpy recovery (ΔH) vs. aging time plot based on the KWW approach. The frequency and temperature-scan effects were eliminated by subtracting the zero-time DSC results from the those obtained for the aged samples [17]. Results showed an increase in the enthalpy of recovery at Tg as the aging time increased in both pure AGM and AGM-Aerosil®300 mixtures, indicating AGM's structural rearrangement leading to equilibrium state.

Fig. 2 shows the effect of aging time on relaxation function, ϕ(t), after fitting to the KWW equation (Eq. (1)) for the neat AGM and AGM-Aerosil®300. In general, it is suggested that non-exponential change of

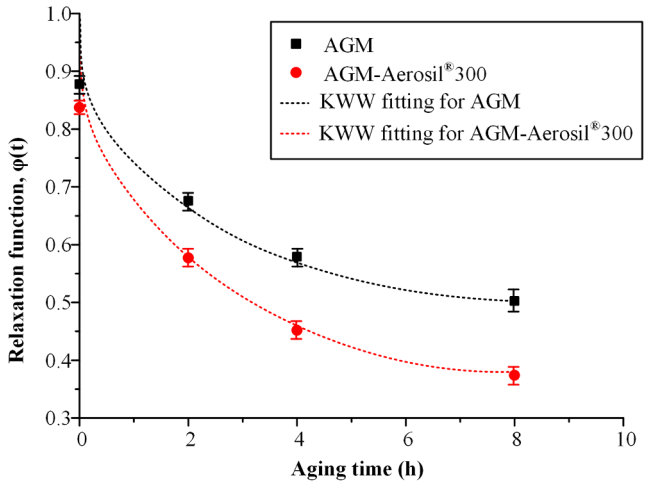

Fig. 2. Effect of annealing (aging time) on the KWW relaxation function φ(t) for AGM and AGM-Aerosil®300.

molecular mobility with temperature indicates the presence of more than one relaxation time [14,47]. This is also verified for the case of AGM and AGM- Aerosil®300 samples where the temperature dependence of φ(t) is fitted well by the KWW equation.

Results showed that AGM alone and AGM – Aerosil®300 binary systems exhibit different relaxation behavior. Specifically, the KWW relaxation time for AGM was $8.49x10^4$ s compared to $2.90 * 10^4$ for AGM- Aerosil®300, while the calculated β values were 0.39 and 0.37 for AGM and AGM – Aerosil®300, respectively. Hence, considering that amorphous systems with the smallest relaxation time have the largest molecular mobility and tend to recrystallize faster, the above results indicate that the presence of Aerosil®300 (even at low amounts, i.e. 5.0% w/w) results in reduced AGM molecular mobility. In regards to β, values for fragile glass forming compounds such as AGM, are generally recorded between 0.3 and 0.8, indicating a significant distribution of relaxation times [14,48].

In a further step, in order to properly compare the relaxation rates of the two examined systems (i.e. AGM and AGM – Aerosil®300) the stretched relaxation time constant, τ^{β}, was calculated (Table 1) as it shows lower sensitivity to experimental error [35]. Results showed τ^{β} values of 83.61 and 44.78, for AGM and AGM – Aerosil®300, respectively, indicating a nearly two-fold reduction in stretched relaxation times when Aerosil is added into the mixture.

3.1.1.2. AG fitting. Fig. 3 shows the DSC thermograms along with corresponding Arrhenius plots of the heating rate dependence for both AGM and AGM - Aerosil®300 samples during the evaluation of relaxation time via AG approach. Results showed that in both cases the DSC enthalpic overshoot at Tg increases as the heating rate increases. Additionally, a good linear fit (coefficient of determination, R^2, values above 0.96) was observed between the logarithm of the selected DSC heating rates (lnq) and the inverse values of the glass transition temperature (1/Tg) for both AGM and AGM – Aerosil®300

Table 1
Kinetic parameters of amorphous AGM and AMG – Aerosil®300 samples during evaluation of relaxation time by fitting of the KWW and AG equations.

Parameter	AGM	AGM- Aerosil®300
D (AG-fitting)	41.6	35.8
T_o (AG-fitting) [K]	127.1	137.3
β (KWW fitting)	0.39	0.37
τ (KWW) [s]	8.49×10^4	$2.90 * 10^4$
τ^{β} (KWW)	83.61	44.78
τ^0 (AG) [s]	112.3	150.2

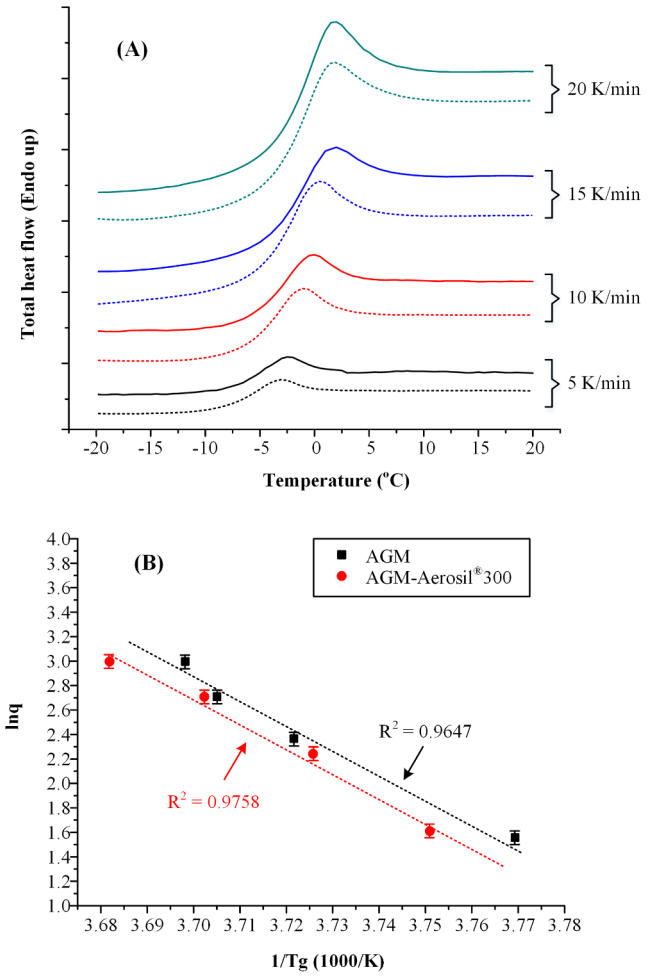

Fig. 3. (A) DSC thermograms (full line depicts AGM while dashed lines depict AGM – Aesosil®300 mixtures); and (B) Arrhenius plot of the heating rate dependence during relaxation time determination experiments using the AG equation.

samples. However, the different Tg dependency on heating rate for pure API and API – Aerosil®300 samples, indicated by the slope of the fitting lines in Fig. 3**B**, suggested different amorphous phase related properties.

Table 1 summarizes the AG fitting parameters. In general, the deviation from the linear Arrhenius behavior as a function of temperature is described by parameters D (which is a measure of fragility) and T_o. As the value of the strength parameter (D) decreases, the molecular mobility slows down (greater initial relaxation time), while T_o indicates the temperature of zero configurational entropy. In the case of pure AGM, a D value of 41.6 indicated that the amorphous API has a strong glass forming behavior, while the addition of Aerosil®300 led to a decrease in strength parameter (D = 35.8) suggesting that the addition of silica reduces API's molecular motion. Additionally, results for T_o values (127.1 K (i.e. −151.3 °C) and 137.3 (i.e. −135.7 °C) for AGM and AGM-Aerosil®300 samples respectively) indicated that the temperature where all molecular mobility ceases, decreases in the presence of Aerosil®300. Furthermore, results in the same table showed that at Tg both samples show similar relaxation times (τ^0 values in the order to 100 to 150 s).

Fig. 4 shows the estimated initial relaxation time (τ^0) of amorphous AGM and AGM – Aerosil®300 samples as a function of temperature. Results indicated that as the temperature decreases (Tg – T increases) the initial relaxation time of the two samples varies significantly, while, when the temperature of storage decreases, τ^0 values increase

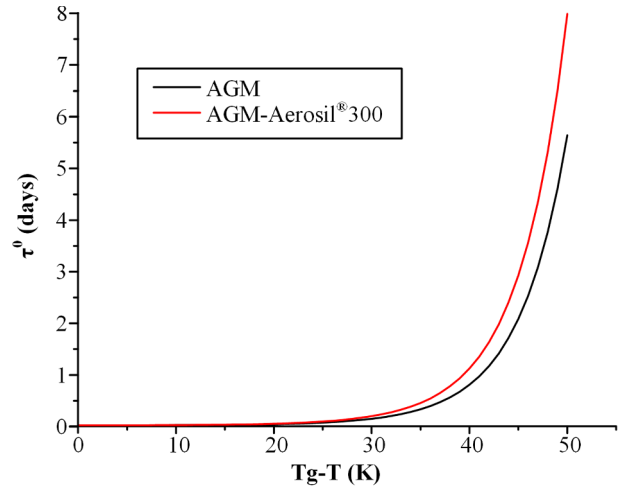

Fig. 4. Estimated initial relaxation times (τ^0) of amorphous AGM and AGM – Aerosil®300 samples as a function of Tg – T by fitting of the AG equation.

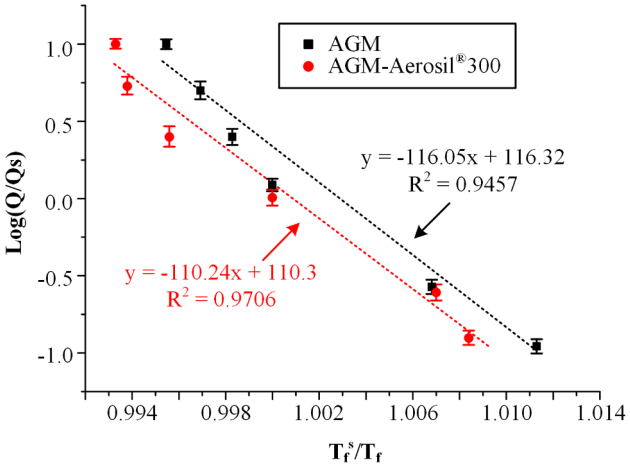

Fig. 5. Scaled Arrhenius plots of the cooling rates vs. the resulting fictive temperatures for the determination of fragility index based on TM-DSC measurements.

exponentially. Generally, in storage temperatures well below Tg, changes in relaxation time are extremely slow and hence, τ^0 values provide a good estimation of the material's molecular mobility [39,46]. Especially, for storage temperatures at 40–50 K below Tg, AGM's initial relaxation time is approximately six (6) days, and hence, it can be said that even in extremely low storage temperatures (i.e. ~50 K below Tg) AGM's molecular motion, expressed in terms τ^0, is not sufficiently suppressed in order to ensure good long-term stability (i.e. 2–3 years). On the other hand, addition of Aerosil®300 shows increased initial relaxation times compared to pure API at the same storage temperature range (τ^0 value reaches 8 days when stored at 50 K below Tg), indicating that in the presence of Aerosil®300 API's molecular motion is reduced. This was in agreement with our previously published storage stability results [20], where amorphous AGM dispersed within a Aerosil®300 matrix was stable when stored for up to one (1) month at 40 °C ± 2 °C/75% RH ± 5%. Comparison, however, of results suggests that, even though the molecular mobility (based on the evaluation of relaxation time) is an important factor of API's physical stability, the increased storage stability of AGM - Aerosil®300 solid dispersions at 40 °C (i.e. ~45 K above API's Tg value) indicates that other factors, such as molecular interactions, devitrification kinetics, and steric hindrance, play an important role in AGM's amorphous phase stabilization. Nevertheless, both approaches followed for the evaluation of AGM's molecular mobility via relaxation time (KWW and AG equations)

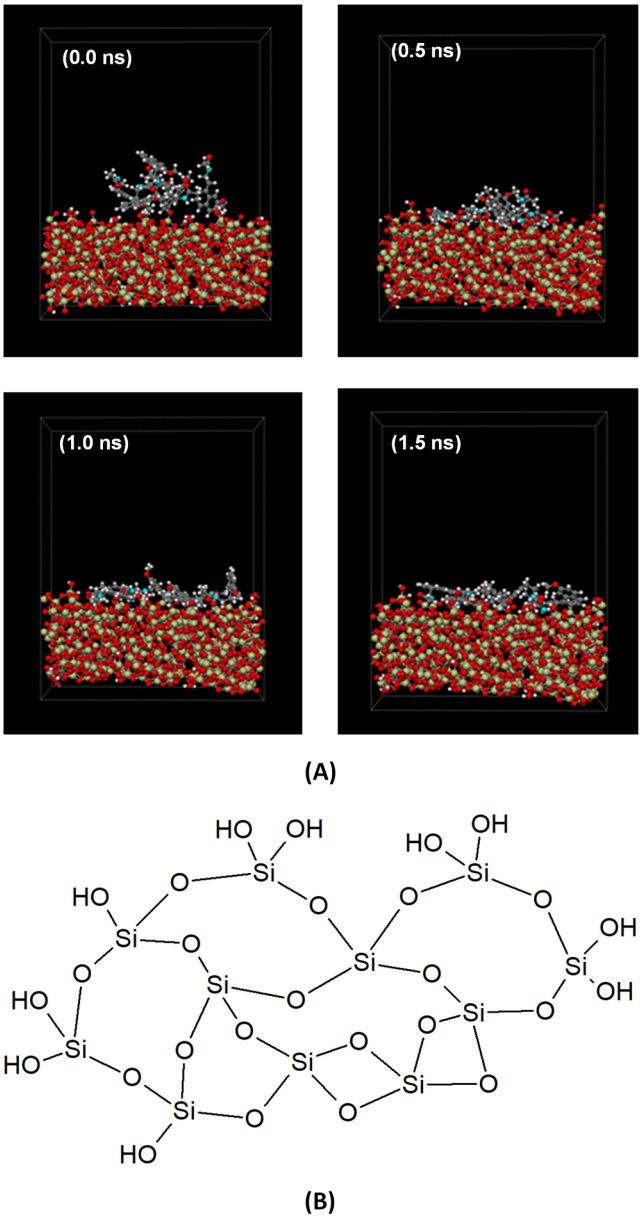

Fig. 6. (A) Snapshots of the molecular dynamics trajectory taken at: 0.0 ns, 0.5 ns, 1.0 ns and 1.5 ns, illustrating the spreading of AGM molecules on the surface of amorphous Aerosil®300. (B) A simple chemical structure of silica surface components used in the simulation process.

showed that even in small amounts (5% w/w) the presence of Aerosil®300 results in a significant reduction of AGM's amorphous phase molecular motion. The presence of intermolecular interaction between AGM and silica as an (additional) mechanism for amorphous AGM stabilization in the presence of Aerosil®300 will be evaluated with the aid of MD simulations and ATR-FTIR spectroscopy in a following section (Section 3.2).

3.1.2. *Fragility via TM-DSC*

Fragility is related to primary diffusive translational and rotational motions of molecules (i.e. *α*-relaxations), which are believed to play a critical role in the crystallization of a material [32]. According to Angell et al. [48] glass-forming liquids are categorized as either "strong" when fragility index, m, is low (≤16) and "fragile" when m is high (≥200). In general, amorphous excipients used for the preparation of pharmaceutical ASD (such as Aerosil®300 which is a covalently bonded inorganic tetrahedrally coordinated material) behave as "strong" glasses

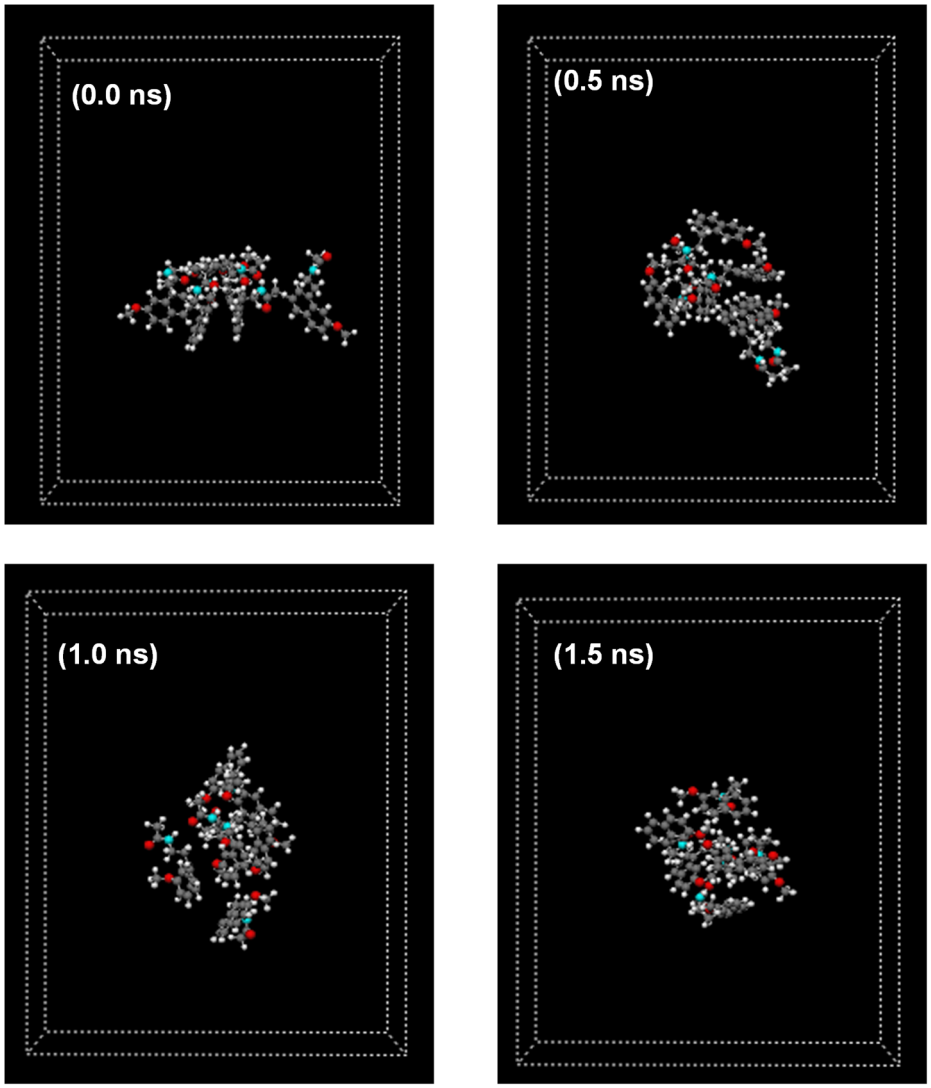

Fig. 7. Snapshots of the molecular dynamics trajectory taken at: 0.0 ns, 0.5 ns, 1.0 ns, and 1.5 ns, illustrating AGM molecular structure without the presence of Aerosil®300.

exhibiting quasi-Arrhenius behavior, while the majority of the low MW active pharmaceutical ingredients are characterized as "moderately fragile" glasses, deviating significantly from Arrhenius behavior around Tg [14,15]. The classification of pharmaceutical glass formers has been reviewed by Yu [49] with strong and fragile glass-formers displaying m values below 40 and above 75, respectively.

TM-DSC scans (data not-shown) resulted in a total heat flow curve which was then divided into reversing (showing glass transition events) and non-reversing (showing enthalpy of recovery for structural relaxation) component. Result showed that in the case of pure AGM the enthalpy of relaxation (ΔH) values increased with decreasing cooling rates (slower cooling leads to increased residence time and hence, increased relaxation), while similar results were obtained also for AGM – Aerosil®300.

Fig. 5 shows the T_f data plotted against the DSC cooling rates based on Eq. (4) for both AGM and AGM – Aerosil®300 samples. T_f values were determined by estimating the difference in ΔH, ΔH(Q), between the standard scan (2 K/min cooling rate) and the rest of the scans performed. Results showed a good linear correlation between the log (Q/Qs) and T_f^s/T_f values with R^2 values of 0.9457 and 0.9706 for AGM and AGM-Aerosil®300, respectively. The fragility indices, expressed by the slope (or the intercept) of the linear fitting curves, were 116.05 for pure AGM and 110.24 for AGM – Aerosil®300 samples, indicating a reduction in the fragility index values when Aerosil®300 is added to AGM.

3.2. Intermolecular interactions: Evaluation via MD simulations and ATR-FTIR spectroscopy

Fig. 6 illustrates snapshots of the molecular dynamics trajectory during the 1.5 ns of the NVT run consisting initially of a "droplet" of six randomly aggregated AGM molecules at the center of the Aerosil®300 surface (the whole simulation process can be seen in the provided video clip), while Fig. 7 shows the same AGM droplet without the presence of Aerosil®300. From the figures, it is seen that only in the presence of Aerosil®300 the AGM molecules consisting the "droplet" spread and attach onto the silica surface by interacting with silanol groups. The same results were obtained in all three MD simulations, indicating good repeatability.

In order to verify this assumption, ATR-FTIR analysis was employed (Fig. 8). Analysis of the FTIR spectra for the two AGM polymorphs (Form I and II) showed high similarity. Specifically, in both cases several characteristic absorption peaks were recorded, corresponding to the stretching vibrations of −N−H, =CH and −C=C (at 3249, 3070, and 1533 cm^{-1}, respectively), the aliphatic chain asymmetrical stretching vibration of $-CH_2$ (at 2940 cm^{-1}), the carbonyl stretching

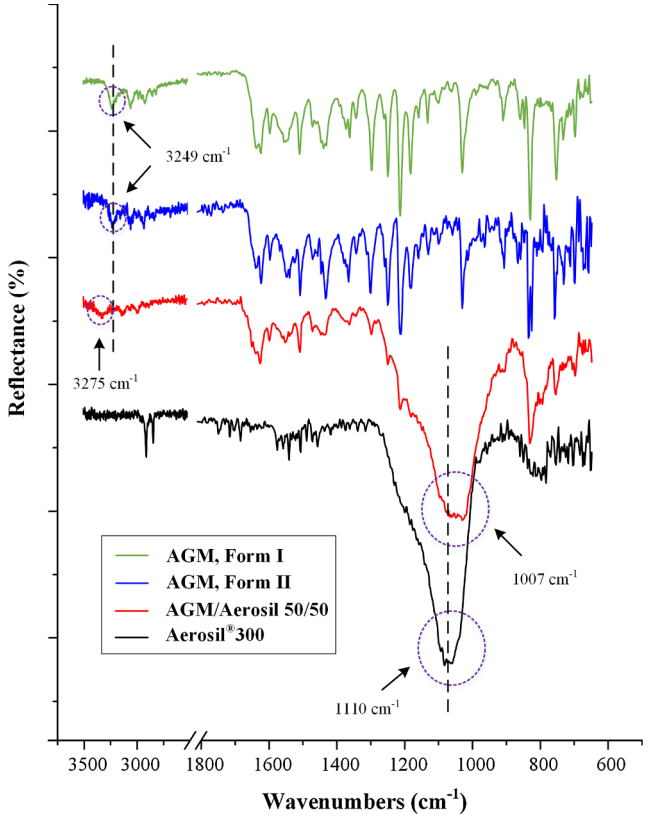

Fig. 8. ATR-FTIR spectra of AGM polymorphs I and II, along with Aerosil®300 and a solid dispersion sample of AGM – Aerosil®300 at 50/50 w/w ratio.

vibration of −C═O (at 1641 cm^{-1}), and the ether bond asymmetrical stretching vibration of C−O−C (at 1215 cm^{-1}) [20]. In regards to Aerosil®300 a broad IR peak was observed at 1110 cm^{-1} due to the antisymmetric Si−O−Si stretching. FT-IR spectrum of the prepared AGM-Aerosil®300 solid dispersion at 50/50 w/w ratio showed a shift in both AGM's −N−H peak from 3249 to 3275 cm^{-1}) and Aerosil's Si_2O peak from 1110 to 1007 cm^{-1}, indicating that an interaction between the two compounds is taking place. This finding verifies the results of MD simulations.

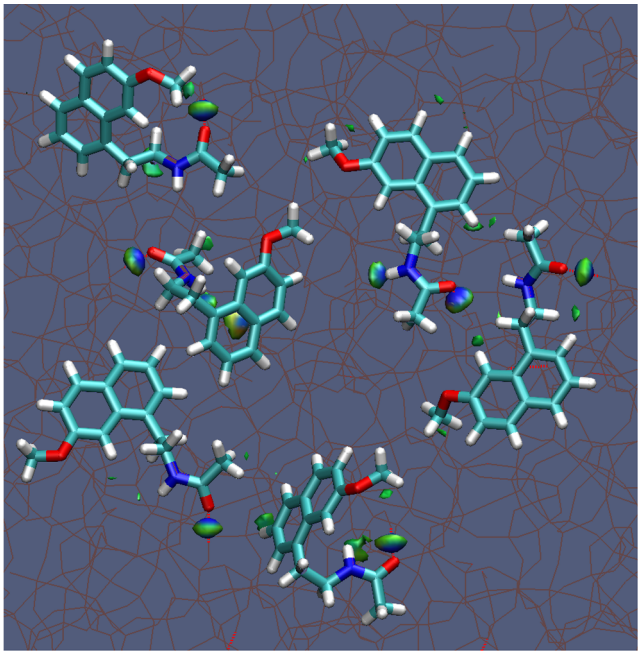

Fig. 10. Representative configurations of agomelatine molecules adsorbed on the surface of amorphous silica (shown in brown), and noncovalent interaction isosurfaces derived from the promolecule electron densities within the independent gradient model.

In a further step, in order to calculate the binding energy between AGM and Aerosil®300, molecular dynamics calculations were performed on a cluster of six molecules of AGM on the surface of amorphous silica, the silica surface, and the cluster of six AGM molecules alone. The energy of each simulation cell at the final point of the

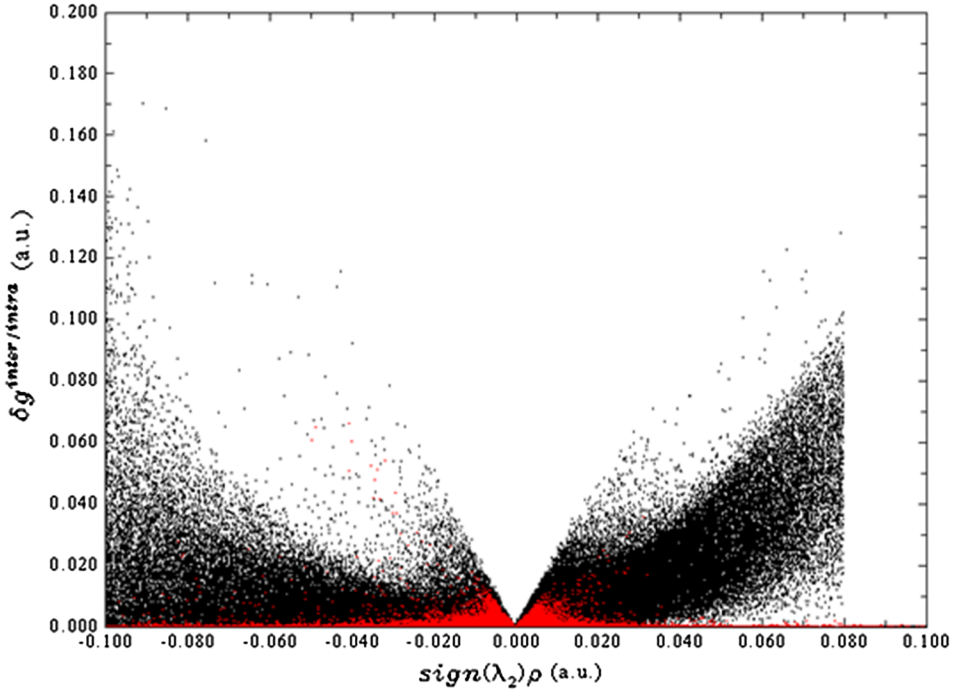

Fig. 9. Scatter plot of δg vs sign(λ_2)ρ indicating regions of intermolecular (red color) and intramolecular (black color) interactions.

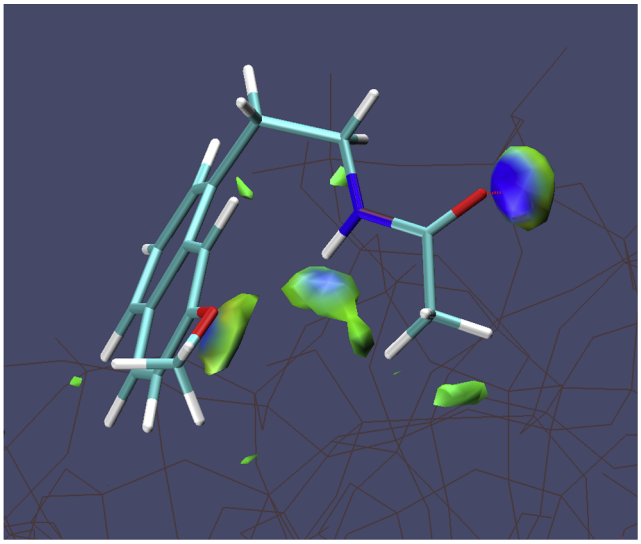

Fig. 11. Close-up illustration of agomelatine molecule interacting with silica (shown in brown) through hydrogen bonds between the C═O and N—H groups, as well as the π-electrons of the resonant ring system.

simulation was calculated after energy minimization, and the binding energy, ΔE_{bind}, (or adsorption energy) was calculated according to Eq. (1):

$$\Delta E_{bind} = E_{total} - (E_{surface} + E_{drug}) \quad (5)$$

where E_{total} is the energy of the AGM-Aerosil®300 cluster (−6287.90 kcal/mol), $E_{surface}$ is the energy of the neat Aerosil®300 surface (−6298.07 kcal/mol) and E_{drug} is the energy of the cluster of six AGM molecules (548.50 kcal/mol). ΔE_{bind} was found to be −538.33 kcal/mol unit cell, or −89.72 kcal/mol when the simulation box contains a single drug molecule.

The nature of the proposed interaction (between AGM and Aerosil®300) was studied in more detail in terms of the independent gradient model [50] which employs calculations of the descriptor δg at the promolecular level:

$$\delta g = |\nabla_{\rho}^{IGMinter}| - |\nabla_{\rho}| \quad (6)$$

where $\nabla_{\rho}^{\text{IGM inter}}$ is the norm of the electron density gradient within the IGM, and ∇_{ρ} is the norm of the electron density gradient of the system. Results of δg are plotted vs the sign(λ_2)ρ, which is the sign of the second density Hessian eigenvalue (λ_2), Fig. 9, and as isosurfaces indicating regions of intermolecular interaction, color-coded according to the value of sign(λ_2)ρ (blue showing strong and attractive, green showing weak interaction and red showing strong and repulsive interaction), Figs. 10 and 11.

From Fig. 9 it is seen that in the negative region of sign(λ_2)ρ there's a small and broad peak of δg not exceeding the value of 0.02, indicating weak intermolecular interactions. The almost symmetrical counterpart at the positive sign(λ_2)ρ range is an indication of the existence of steric repulsion between AGM and Aerosil®300, slightly weaker than the attractive forces.

Indeed, as illustrated in Figs. 10 and 11, AGM's molecules interact mainly through hydrogen bonding between Aerosil®300's silanol O—H, and AGM's acetamide C═O and N—H groups. However, a closer look at the interacting molecules (Fig. 10) reveals interactions between the resonant ring system of AGM and silanol groups, as well as between AGM's methyl group and Aerosil®300's siloxane groups. The red tint present in certain regions of the corresponding isosurfaces indicates steric repulsion.

In sum, MD simulations show that the spreading of AGM on the surface of Aerosil®300 is driven mainly by the hydrogen bonding between silanol and acetamide groups, which was experimentally verified by ATR-FTIR analysis. This interaction along with the reduced AGM's molecular mobility observed in the presence of Aeosil®300 may explain to some extent, the amorphous API formation in Aerosil®300 based solid dispersions and the long term stability of the system observed in our previous work [20].

4. Conclusion

In the current study, molecular mobility and intermolecular interactions were evaluated as two possible mechanisms for pyrogenic silica induced AGM amorphous stabilization. Analysis indicated that the presence of Aerosil®300 results in a reduction of AGM's amorphous phase molecular motion, with fragility index values of 116.05 and 110.24 for pure AGM and AGM-Aerosil®300 dispersions, respectively; while MD simulations revealed the formation of important intermolecular interactions between the two components, which was verified by ATR-FTIR spectroscopy.

Declaration of interest

The authors report no declarations of interest.

Appendix A. Supplementary material

Supplementary data to this article can be found online at https://doi.org/10.1016/j.ejpb.2019.04.015.

References

[1] N. Babu, A. Nangia, Solubility Advantage of Amorphous Drugs and Pharmaceutical Cocrystals, 2011.
[2] P. Barmpalexis, A. Karagianni, K. Kachrimanis, Molecular simulations for amorphous drug formulation: polymeric matrix properties relevant to hot-melt extrusion, Eur. J. Pharm. Sci. 119 (2018) 259–267.
[3] K. Edueng, D. Mahlin, C.A.S. Bergstrom, The need for restructuring the disordered science of amorphous drug formulations, Pharm Res 34 (2017) 1754–1772.
[4] H. Grohganz, P.A. Priemel, K. Lobmann, L.H. Nielsen, R. Laitinen, A. Mullertz, G. Van den Mooter, T. Rades, Refining stability and dissolution rate of amorphous drug formulations, Expert Opin. Drug Del. 11 (2014) 977–989.
[5] G. Van den Mooter, The use of amorphous solid dispersions: a formulation strategy to overcome poor solubility and dissolution rate, Drug Discovery Today: Technologies 9 (2012) e79–e85.
[6] M. Colombo, C. Minussi, S. Orthmann, S. Staufenbiel, R. Bodmeier, Preparation of amorphous indomethacin nanoparticles by aqueous wet bead milling and in situ measurement of their increased saturation solubility, Eur. J. Pharm. Biopharm.: Off. J. Arbeitsgemeinschaft fur Pharmazeutische Verfahrenstechnik e.V 125 (2018) 159–168.
[7] E. Elisei, J.F. Willart, F. Danede, J. Siepmann, F. Siepmann, M. Descamps, Crystalline polymorphism emerging from a milling-induced amorphous form: the case of chlorhexidine dihydrochloride, J. Pharm. Sci. 107 (2018) 121–126.
[8] M. Rams-Baron, R. Jachowicz, E. Boldyreva, D. Zhou, W. Jamroz, M. Paluch, Amorphous Drugs: Benefits and Challenges, Springer International Publishing, 2018.
[9] L.S. Taylor, S.L. Shamblin, Amorphous Solids, in: H.G. Brittain (Ed.), Polymorphism in Pharmaceutical Solids, Informa Healthcare USA Inc, 2009.
[10] C. Bhugra, R. Shmeis, S.L. Krill, M.J. Pikal, Different measures of molecular mobility: comparison between calorimetric and thermally stimulated current relaxation times below Tg and correlation with dielectric relaxation times above Tg, J. Pharm. Sci. 97 (2008) 4498–4515.
[11] S. Yoshioka, Y. Aso, Correlations between molecular mobility and chemical stability during storage of amorphous pharmaceuticals, J. Pharm. Sci. 96 (2007) 960–981.
[12] S.L. Shamblin, X. Tang, L. Chang, B.C. Hancock, M.J. Pikal, Characterization of the time scales of molecular motion in pharmaceutically important glasses, J. Phys. Chem. B 103 (1999) 4113–4121.
[13] B.C. Hancock, S.L. Shamblin, G. Zografi, Molecular mobility of amorphous pharmaceutical solids below their glass transition temperatures, Pharm. Res. 12 (1995) 799–806.
[14] G. Zografi, A. Newman, Interrelationships between structure and the properties of amorphous solids of pharmaceutical interest, J. Pharm. Sci. 106 (2017) 5–27.
[15] P. Chakravarty, K. Pandya, K. Nagapudi, Determination of fragility in organic small molecular glass forming liquids: comparison of calorimetric and spectroscopic data and commentary on pharmaceutical importance, Mol. Pharm. 15 (2018) 1248–1257.
[16] C.A. Angell, Perspective on the glass transition, J. Phys. Chem. Solids 49 (1988) 863–871.

[17] P. Ke, S. Hasegawa, H. Al-Obaidi, G. Buckton, Investigation of preparation methods on surface/bulk structural relaxation and glass fragility of amorphous solid dispersions, Int. J. Pharm. 422 (2012) 170–178.
[18] V. Srinivasan, R. Zakaria, Z. Othman, E.C. Lauterbach, D. Acuna-Castroviejo, Agomelatine in depressive disorders: its novel mechanisms of action, J. Neuropsys. Clin. Neurosci. 24 (2012) 290–308.
[19] Y. Liu, L. Chen, Y. Ji, Quantification and structural elucidation of potential impurities in agomelatine active pharmaceutical ingredient, J. Pharm. Biomed. Anal. 81–82 (2013) 193–201.
[20] P. Barmpalexis, A. Grypioti, E. Vardaka, A. Karagianni, K. Kachrimanis, Development of a novel amorphous agomelatine formulation with improved storage stability and enhanced bioavailability, J. Pharm. Sci. 107 (2018) 257–266.
[21] C.A. McCarthy, R.J. Ahern, K.J. Devine, A.M. Crean, Role of drug adsorption onto the silica surface in drug release from mesoporous silica systems, Mol. Pharm. 15 (2018) 141–149.
[22] D.L. Evans, S.V. King, Random network model of vitreous silica, Nature 212 (1966) 1353.
[23] E.F. Vansant, P. Van Der Voort, K.C. Vrancken, Chapter 3 The surface chemistry of silica, in: E.F. Vansant, P. Van Der Voort, K.C. Vrancken (Eds.), Studies in Surface Science and Catalysis, Elsevier, 1995, pp. 59–77.
[24] L.T. Zhuravlev, The surface chemistry of amorphous silica, Zhuravlev model, Colloid Surfaces A: Physicochem. Eng. Aspects 173 (2000) 1–38.
[25] W. Gonçalves, J. Morthomas, P. Chantrenne, M. Perez, G. Foray, C.L. Martin, Molecular dynamics simulations of amorphous silica surface properties with truncated Coulomb interactions, J. Non-Cryst. Solids 447 (2016) 1–8.
[26] J. Samela, S.A. Norris, K. Nordlund, M.J. Aziz, Optimization of large amorphous silicon and silica structures for molecular dynamics simulations of energetic impacts, Nucl. Instrum. Methods Phys. Res. Section B: Beam Interact. Mater. Atoms 269 (2011) 1568–1571.
[27] F.S. Emami, V. Puddu, R.J. Berry, V. Varshney, S.V. Patwardhan, C.C. Perry, H. Heinz, Force field and a surface model database for silica to simulate interfacial properties in atomic resolution, Chem. Mater. 26 (2014) 2647–2658.
[28] P. Ugliengo, M. Sodupe, F. Musso, I.J. Bush, R. Orlando, R. Dovesi, Realistic models of hydroxylated amorphous silica surfaces and MCM-41 mesoporous material simulated by large-scale periodic B3LYP calculations, Adv. Mater. 20 (2008) 4579–4583.
[29] H. Heinz, T.-J. Lin, R. Kishore Mishra, F.S. Emami, Thermodynamically consistent force fields for the assembly of inorganic, organic, and biological nanostructures: the INTERFACE force field, Langmuir, 29 (2013) 1754–1765.
[30] H. Heinz, Adsorption of biomolecules and polymers on silicates, glasses, and oxides: mechanisms, predictions, and opportunities by molecular simulation, Curr. Opin. Chem. Eng. 11 (2016) 34–41.
[31] H. Heinz, H. Ramezani-Dakhel, Simulations of inorganic–bioorganic interfaces to discover new materials: insights, comparisons to experiment, challenges, and opportunities, Chem. Soc. Rev. 45 (2016) 412–448.
[32] V. Caron, C. Bhugra, M.J. Pikal, Prediction of onset of crystallization in amorphous pharmaceutical systems: phenobarbital, nifedipine/PVP, and phenobarbital/PVP, J. Pharm. Sci. 99 (2010) 3887–3900.
[33] P. Karmwar, K. Graeser, K.C. Gordon, C.J. Strachan, T. Rades, Investigation of properties and recrystallisation behaviour of amorphous indomethacin samples prepared by different methods, Int. J. Pharm. 417 (2011) 94–100.
[34] K.A. Graeser, J.E. Patterson, T. Rades, Applying thermodynamic and kinetic parameters to predict the physical stability of two differently prepared amorphous forms of simvastatin, Curr. Drug Deliv. 6 (2009) 374–382.
[35] J. Liu, D.R. Rigsbee, C. Stotz, M.J. Pikal, Dynamics of pharmaceutical amorphous solids: the study of enthalpy relaxation by isothermal microcalorimetry, J. Pharm. Sci. 91 (2002) 1853–1862.
[36] G. Van den Mooter, P. Augustijns, R. Kinget, Stability prediction of amorphous benzodiazepines by calculation of the mean relaxation time constant using the Williams-Watts decay function, Eur. J. Pharm. Biopharm.: Off. J. Arbeitsgemeinschaft fur Pharmazeutische Verfahrenstechnik e.V 48 (1999) 43–48.
[37] G. Adam, J.H. Gibbs, On temperature dependence of cooperative relaxation properties in glass-forming, Liquids (1965).
[38] L. Olivares-Quiroz, L.S. Garcia-Colin, Evidence of α fluctuations in myoglobin's denaturation in the high temperature region: average relaxation time from an Adam-Gibbs perspective, Biophys. Chem. 144 (2009) 123–129.
[39] C. Mao, S. Prasanth Chamarthy, S.R. Byrn, R. Pinal, A calorimetric method to estimate molecular mobility of amorphous solids at relatively low temperatures, Pharm Res 23 (2006) 2269–2276.
[40] L. Wang, V. Velikov, C. Angell, Direct determination of kinetic fragility indices of glassforming liquids by differential scanning calorimetry: Kinetic versus thermodynamic fragilities, 2002.
[41] A.K. Rappe, W.A. Goddard, Charge equilibration for molecular dynamics simulations, J. Phys. Chem. 95 (1991) 3358–3363.
[42] W. Van Gunsteren, A. Mark, Validation of molecular dynamics simulation, J. Chem. Phys. 108 (1998) 6109–6116.
[43] W. Humphrey, A. Dalke, K. Schulten, VMD: visual molecular dynamics, J. Mol. Graph. 14 (1996) 33–38.
[44] T. Lu, F. Chen, Multiwfn: a multifunctional wavefunction analyzer, J. Comput. Chem. 33 (2012) 580–592.
[45] M. Yoshioka, B.C. Hancock, G. Zografi, Crystallization of indomethacin from the amorphous state below and above its glass transition temperature, J. Pharm. Sci. 83 (1994) 1700–1705.
[46] C. Mao, S.P. Chamarthy, R. Pinal, Calorimetric study and modeling of molecular mobility in amorphous organic pharmaceutical compounds using a modified Adam-Gibbs approach, J. Phys. Chem. B 111 (2007) 13243–13252.
[47] M.T. Cicerone, M.D. Ediger, Enhanced translation of probe molecules in supercooled o-terphenyl: signature of spatially heterogeneous dynamics? J. Chem. Phys. 104 (1996) 7210–7218.
[48] C. Angell, K. Ngai, G. McKenna, P. McMillan, S.W.J. Martin, Relaxation in glass forming liquids and amorphous, Solids (2000).
[49] L. Yu, Amorphous pharmaceutical solids: preparation, characterization and stabilization, Adv. Drug Deliv. Rev. 48 (2001) 27–42.
[50] C. Lefebvre, G. Rubez, H. Khartabil, J.-C. Boisson, J. Contreras-García, E. Hénon, Accurately extracting the signature of intermolecular interactions present in the NCI plot of the reduced density gradient versus electron density, PCCP 19 (2017) 17928–17936.